Phytoplankton community succession and dynamics using optical approaches

Glaucia M. Fragoso [a,*], Geir Johnsen [a,b], Matilde S. Chauton [c], Finlo Cottier [d,e], Ingrid Ellingsen [c]

[a] Centre of Autonomous Marine Operations and Systems (AMOS), NTNU,Trondheim Biological Station, Dept. Biology, Norwegian University of Science and Technology (NTNU), Trondheim, Norway
[b] University Centre in Svalbard (UNIS), Longyearbyen, Norway
[c] SINTEF Ocean, Dept. Env. & New Resources, 7465, Trondheim, Norway
[d] Scottish Association for Marine Science (SAMS), Argyll, United Kingdom
[e] Dept. of Arctic and Marine Biology, UiT the Arctic University of Norway, Tromsø, Norway

ARTICLE INFO

ABSTRACT

The phytoplankton in coastal regions are responding to constant environmental changes, thus the use of proxies derived from *in situ* frequent time-series observations and validated from traditional microscopic or pigment methods can be a solution for detecting rapid responses of community dynamics and succession. In this study, we combined *in situ* high-frequency (every 30 min from May to September 2017) optical and hydrographic data from a moored buoy and weekly discrete samplings to track phytoplankton community dynamics and succession in Mausund Bank, a highly productive region of the coast of Norway. Three hydrographic regimes were observed: mixing period (MP) in spring, onset of stratification (transient period, TP) in summer and a stratified period (SP) in fall, with occasional strong winds that disrupted the surface stratification in the beginning of September. A bloom dominated by the diatom *Skeletonema costatum* was observed in the MP due to intense mixing and nutrient availability, while flagellates prevailed in nutrient-poor waters during the TP, followed by a bloom dominated by rhizosolenid diatoms (*Proboscia alata* and *Guinardia delicatula*), when stratification peaked. A mixed assemblage of diatoms (e.g. *Pseudo-nitzschia*), coccolithophores and dinoflagellates occurred during the SP, as strong winds reintroduced nutrients to surface waters. Through pigment (chemotaxonomy) and microscopic observations, we tested, for the first time in a coastal region, whether an 'optical community index' derived from *in situ* measurements of chlorophyll *a* fluorescence (*Fchla*) and optical particulate backscattering (*bbp*) is suitable to differentiate between diatom versus flagellate dominance. We found a negative relationship between *Fchla:bbp* and diatom:flagellate, contrary to previous observations, possibly because of the influence of non-algal contribution (e.g. zooplankton, fecal pellets and detritus) to the *bbp* pool in highly productive systems. This finding suggests that such relationship is not universal and that other parameters are needed to refine the optical community index in coastal regions.

1. Introduction

Marine phytoplankton communities rapidly respond to short- (e.g. diurnal and tidal fluctuations), seasonal (e.g. water column stability, temperature, photoperiod) and long-term (e.g. climate-induced) environmental changes (Beaugrand et al., 2002; Blauw et al., 2012). Changes in the community composition and function of primary producers impact energy transfer to the upper trophic layers and global biogeochemical cycles (Beaugrand et al., 2002).

The plankton in coastal regions are responding to constant disturbances, which impose a persistent pressure for each species to compete over resources and/or acclimate and adapt to the new conditions (Blauw et al., 2012). Hydrographic forcing (advective currents, storm events, upwelling, tides, fronts and eddies) occurring on the scale of hours to days and irregular bathymetry (particularly at shallow bank areas) frequently alter the physical environment in coastal regions (Fragoso et al., 2019a). Seasonality, mainly in temperate and high latitudinal coastal zones, is also known to drive phytoplankton community succession, since the balance between mechanical mixing (winter mixing, seasonal storms) and stratification (thermally- or haline-driven, e.g.

---

ice melt, riverine input) changes throughout the year (Edwards et al., 2013). The degree of physical disturbance (in terms of severity and frequency) and its seasonal variability determine phytoplankton species succession, the state of community organization and diversity in these areas (Reynolds, 1993).

Because plankton can rapidly respond to environmental variability (e.g. light, temperature and nutrients), time-series measurements with high temporal resolution (e.g. sub-hourly) are needed to study the fluctuation of community composition in coastal, highly dynamic environments (Martin-Platero et al., 2018). Analyses of plankton samples via traditional microscopic approaches are, however, challenging because they are time-consuming, limiting the number of samples that can be processed and, thus, the temporal resolution that can be realistically achieved. For this reason, *in situ* techniques that capture fine-scale temporal trends in plankton communities are necessary to monitor rapid changes and understand community dynamics. Such techniques include enabling automated (pre-defined settings, e.g. imaging flow cytometer, Fragoso et al. (2019b)) and autonomous technologies ('trained' to make its own decisions via machine learning, e.g. silhouette camera (Davies and Nepstad, 2017; Fossum et al., 2019; Fragoso et al., 2019a) for plankton quantification and identification. While *in situ* techniques are necessary, taxonomic investigations using conventional approaches (microscopic and pigment-based) are still important for data validation.

Bio-optical techniques are often used for *in situ* detection of plankton taxonomic groups and function based on their optical fingerprint (pigment composition, *in vivo* spectral absorption, reflectance, fluorescence and scattering) and ecological significance (autotrophic versus heterotrophic roles using flow cytometry, for example) (Pereira et al., 2017). Many field observations of phytoplankton are based on optical signals either directly from the cells (e.g. chlorophyll *a* fluorescence, *Fchla*) or measurements of backscattered light, which is modulated by the interaction of light with cells in the water (Lehmuskero et al., 2018). Recently, a simplistic approach that uses the ratio of *Fchla* (as a proxy for chlorophyll *a* concentration [*Chl a*]) to particulate backscattering coefficient (*bbp*) from sensors attached to moored buoys and gliders has been suggested to differentiate diatom- and flagellate-dominated communities (Cetinić et al., 2012, 2015). In addition to group-specific taxonomic segregation, deviations of patterns of *Fchla* and *bbp*, which generally covary in a power relationship, have been attributed to changes in photo-acclimation or the contribution of non-algal particles (Barbieux et al., 2017). This proxy has successfully explained changes in community composition in open, clear waters, non-dominated by coccolithophores (which highly contribute to backscattering) (Cetinić et al., 2015). However, it is still necessary to investigate the *Fchla:bbp* approach for determining community composition in coastal waters to fully understand its applications and limitations in marine systems.

In this study we track the community dynamics and succession in a biological hotspot near the Frøya island in the Froan archipelago (highly productive region) at the coast of mid-Norway. The goals are to study the hydrodynamic impact on phytoplankton community and species succession in a biological hot-spot and to investigate whether an optical index is suitable to determine *in situ* functional groups (diatoms and flagellates) ratios. We combined pigment characteristics (chlorophylls and carotenoids from discrete water samples) and *in situ* optical detection of *Fchla* and *bbp* from a moored buoy to identify the phytoplankton functional groups (diatoms versus flagellates). We used high-frequency (temporal resolution of 30 min) time-series hydrographical and optical data from sensors, ideal for detecting rapid temporal change, with discrete water sampling of phytoplankton taxonomy (microscopic and pigment-based) to validate our findings. This study uniquely provides the basis for understanding the relationship between *Fchla* and *bbp* variations and phytoplankton community structure in coastal regions and can be applicable to other highly productive and dynamic ecosystems.

2. Methods

2.1. Study area

The Mausund Bank area (63.8°- 64.2°N, 8.2°–9.0° E) is located in the Froan archipelago, off the coast of mid-Norway. This area was chosen for our study because it is considered a dynamic biological hotspot where shallow irregular bathymetry, wind, tidal mixing and internal waves sustain high levels of primary productivity and biological diversity (Fragoso et al., 2019a). The dominant oceanic currents are the Norwegian Coastal Current (NCC) and the North Atlantic Current (NAC). The NCC is a surface water mass that flows northwards along the coast of Norway and consists of a mixture of brackish water from the Baltic and freshwater runoff from the Norwegian fjords (Skagseth et al., 2011). The main flow of NAC brings warm, saline and nutrient-rich Atlantic Water (AW) along the shelf break with side branches bringing AW on to the shelf underneath the fresher NCC. This water may reach the surface through coastal upwelling or can occasionally intrude onto the bank via internal waves (Fragoso et al., 2019a).

2.2. Buoy sampling

An oceanographic moored buoy with sensors (see below) was deployed at the edge of Mausund Bank (63° 57′ 48.9″ N, 8° 37′ 53.4″ E, ~150 m deep) for time series data collection (sample interval 30 min) from 16th May - 15th September 2017 (Fig. 1). *In situ Fchla* ($\lambda_{ex} = 470$ nm, $\lambda_{em} = 695$ nm) was used to estimate [*Chl a*] in mg m^{-3} and optical particulate backscattering coefficient at 700 nm measured at an angle, Θ, of 124° to estimate *bbp* in m^{-1} with an Eco Triplet BBFL2 sensor (Wet Labs, Oregon, USA). Both sensors were placed at 3 m depth. Atmospheric downwelling irradiance (*E*) in the Photosynthetically Active Radiation (*PAR*) range (E_{PAR}, 400–700 nm) was measured by an irradiance collector (2pi, 180°), ECO PAR sensor (Wet Labs, Oregon, USA), mounted at the top of the buoy, 3 m above sea surface. Conductivity (to calculate salinity)–temperature–depth (CTD) sensors (Aanderaa Instruments, Norway) were placed at 1, 10, 30 and 60 m depth. An Acoustic Doppler Current Profiler (ADCP, Aquadopp Profiler 400 kHz, Nortek, Norway) was placed downward-looking at 0.75 m depth and used to measure current direction and speed every 2 m down to 40 m depth. All sensors were factory-calibrated prior to buoy deployment. Data from the buoy were transferred in near real-time to the SINTEF SSO laboratory facility via mobile phone network.

2.3. Field work and water sampling

CTD casts and water samples for hydrographic, nutrient and biological analyses were collected, on average, every 7 days (varying from 3 to 12 days between sampling) at two different locations at Mausund Bank. One station was within the bank (station A) and the other station at the northern edge of the bank, near the moored buoy (station B) (Fig. 1). Sampling occurred mostly during rising or high tide, unless weather conditions made it unfeasible. Photoperiod (day length in hours) was calculated based on the geographical coordinates of Mausund Bank and sampling date using the NOAA Solar Calculator website (https://www.esrl.noaa.gov/gmd/grad/solcalc/). Table S1 (supplementary material) shows the dates, distinct tidal conditions and photoperiod at each sampling time.

Simultaneously with water sampling, a CTD (SD204 model, SAIV A/S, Norway) was deployed on a winch at the side of the boat, where vertical profiles from the surface down to 100–150 m at each station were performed. To determine water column stability, the Brunt-Väisälä frequency (N^2, s^{-1}), which represents the rate of the angular velocity at which a small perturbation of the stratification will re-equilibrate, was calculated from the CTD upcasts (Mojica et al., 2015). For this, we used the Matlab function *sw_bfrq* from the SEAWATER package (v.3) provided by the CSIRO (www.cmar.csiro.au).
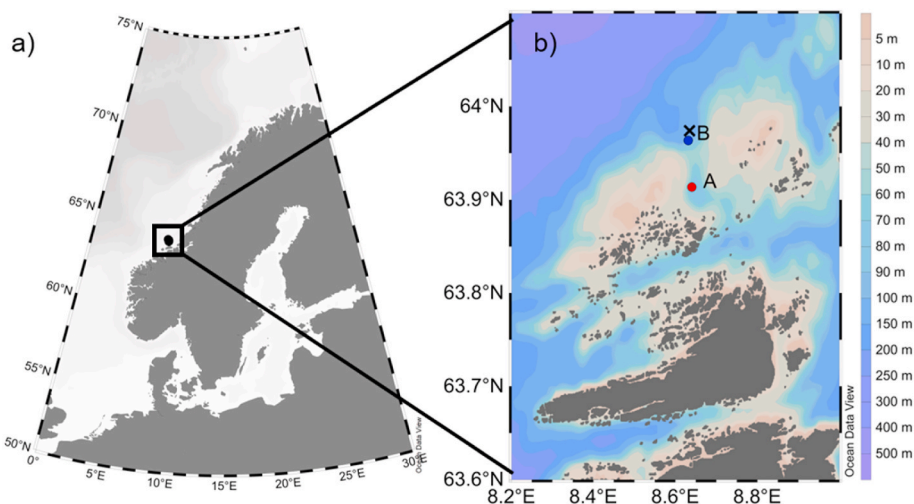
Fig. 1. Map showing the a) Froan archipelago in the coast of Norway and b) the area of Mausund, where stations were sampled within the bank (A) and at the edge of the bank (B) for discrete water sampling and where a mooring buoy with several sensors was placed (near station B, cross symbol).

Water samples were collected using a 2.5 L built-in water sampler at stations A and B at 5 and 15 m. Samples were collected for [*Chl a*] and other pigments, nutrients, particulate organic carbon (*POC*) and plankton identification and enumeration. Net tows (mesh size 20 μm) were performed close to the surface (<15 m) for phytoplankton identification and the concentrates from the net were fixed with formaldehyde to a final concentration of 4%. Lugol-fixed samples (neutral, ~2–3% final concentration) were stored cold (4 °C) and in the dark for later microscopy in the laboratory.

Nutrient samples were filtered with 0.8 μm polycarbonate filter to remove particles, collected in centrifuge tubes and frozen to −20 °C for laboratory analyses. Nutrient concentrations (nitrite plus nitrate [NO_2+ NO_3], hereafter referred to as nitrate [NO_3], silicate [SiO_4], phosphate [PO_4] and ammonium [NH_4]), were determined using a continuous flow automated analyzer (CFA, Auto Analyzer 3, SEAL).

For pigment analyses, 0.5 L – 2 L of water were immediately filtered (depending on biomass) onto a 25 mm Whatman GF/F glass fiber filter. After filtration, each filter was double-folded, wrapped in aluminum foil and placed into the freezer at −20 °C for later analyses in the laboratory.

For *POC* analyses, water was filtered (1 L – 2 L) onto a pre-combusted 25 mm Whatman GF/F glass fiber filter and immediately inserted in cryovials and stored at −20 °C for later analyses.

2.4. Buoy data correction and indices

A Stratification Index (*SI_buoy*, kg m^{-4}) was calculated from the buoy CTD measurements (from May to September 2017) to quantify water column stratification in the upper layer (10–60 m). *SI_buoy* was calculated as the maximum daily density (σ_θ) difference between 10 m and 60 m divided by the difference in depth (50 m) (Fragoso et al., 2016).

Wind stress (τ) is calculated from wind speed (W_s) measurements from the buoy as $\tau = \rho C_d W_s^2$, where $\rho = 1.2$ kg m^{-3} is the air density and C_d is the drag coefficient calculated as

$$C_d = 10^{-3} * \begin{cases} 1.14, & W_s \leq 10 \\ 0.49 + 0.065W_s, & W_s > 10 \end{cases}$$

The formulation is from Large and Pond (1981) based on wind speed at 10 m height. The wind measurements at the buoy was at approximately 3 m height.

Light scattering measurements from the Eco Triplet sensor were converted to volume scattering function of particles (β_p, 700 nm) by subtracting the volume scattering function of the seawater (β_{sw}) from the total volume scattering function (β_{total}, 700 nm) from the volume scattering function of the seawater (β_{sw}), previously calculated in Zhang

et al. (2009). To obtain the particulate light backscattering coefficient (*bbp*, m^{-1}), β_p (700 nm) was multiplied by $2\pi\chi$, using a χ factor of 1.077, according to Sullivan et al. (2013).

In situ Fchla data from the buoy were first corrected for non-photochemical quenching (*NPq*) occurrences. *NPq* is a mechanism by which live cells exposed to high light levels dissipate excess energy as heat (Huot and Babin, 2010). Empirically, *NPq* is manifested as a reduction in *Fchla* signal during the daytime hours, with maximum quenching (reduction) of *Fchla* signal occurring around noon and at the surface (Roesler et al., 2017). To correct for *NPq*, *Fchla* observations from times which E_{PAR} exceeded 200 μmol photons m^{-2} s^{-1} were excluded according to Roesler et al. (2017). Data that were compromised by biofouling on sensor windows (microphytobentos), which were identified by an exponential increase of *Fchla* and *bbp* coefficient signal to values considered out of range over a short period (hours), were removed from the analysis according to Roesler (2016). To reduce the variability of the data, a median of 7 consecutive points was calculated as in Cetinić et al. (2015). A list of parameters measured from the sensors and platforms as well as their symbology is described in Table 1.

2.5. Pigment analyses

Fluorometric [*Chl a*] that were determined *in vitro* are here defined as [*Chla_in-vitro*]. This used a non-acidification method (Holm-Hansen and Riemann, 1978) with a Turner Designs Trilogy fluorometer (model: 7200-000) after 2 h extraction at −10 °C in 100% methanol. Additionally, pigments were quantified using a reverse-phase High Performance Liquid Chromatography (HPLC) (Hewlett-Packard 1100 Series system) equipped with a diode array detector (spectral absorbance) and a Symmetry C8 column for pigment separation. The method used is described in Rodríguez et al. (2006) after modification from Zapata et al. (2000). Frozen filters were extracted for at least 24 h at −20 °C in 100% methanol and extracts were re-filtered through Millipore 0.45 μm syringe filters to remove debris before injection into the HPLC system. HPLC calibration, specific extinction coefficients used for pigment quantification and limits of detection are reported in Fragoso et al. (2019a).

2.6. Pigment interpretation and CHEMTAX

The CHEMTAX software (version 1.95, Mackey et al., 1996) estimates the quantitative [*Chl a*] (here defined as *Chla_CHEMTAX*) of distinct phytoplankton groups based on assumed ratios of accessory pigments to [*Chl a*] from the literature. This software utilizes a factorization program

Table 1

List of measured variables from different platforms (boat or buoy), their symbology and methodologies.

Parameter measured/ calculated	Unit	Symbol	Instrument/plataform	
			Boat	Buoy
Temperature, Salinity estimated from conductivity	°C	T, S	STD/CTD SD204 (SAIV/AS)	CTD (Aanderaa)
In situ chlorophyll *a* fluorescence	mg m^{-3}	*Fchla*		Eco Triplet BBFL2 (Wet Labs)
In situ volume scattering function, calculated particulate backscattering coefficient	m^{-1}	*β700, bbp*		Eco Triplet BBFL2 (Wet Labs)
Irradiance	μ mol photons m^{-2} s^{-1}	E_{PAR}		ECO PAR (Wet Labs)
Acoustic Doppler Current Profiler	*ADCP*			Aquadopp (Nortek)
Brunt-Väisälä Frequency	s^{-1}	N^2	STD/CTD SD204 (SAIV/AS)	
Wind Stress	N m^{-2}	*τ*		
Stratification Index from buoy measurements	kg m^{-4}	SI_{buoy}		CTD (Aanderaa)
Integrated E_{PAR} values at 60 m	μ mol photons m^{-2} s^{-1} kg m^{-4}	$SI_{buoy}*E_{PAR}$		
Nutrient concentrations: Nitrate, phosphate, silicate, ammonium	μM	$[NO_3]$, $[PO_4]$, $[SiOH_4]$, $[NH_4]$		
In vitro chlorophyll *a* extract	mg Chla m^{-3}	$Chla_{in-vitro}$	Turner design	
In vitro chlorophyll *a* extract	mg Chla m^{-3}	$Chla_{HPLC}$	HPLC	
Xanthophyll pigments per chlorophyll *a*		$(DD+DT)/Chla_{HPLC}$		
De-epoxidation state of xanthophyll		$DT/(DD+DT)$		
Chlorophyll *a* biomass per algal group	mg Chla m^{-3}	$Chla_{CHEMTAX}$	Derived from CHEMTAX	
Particulate organic carbon	mg m^{-3}	*POC*		
Carbon biomass per algal group	mg m^{-3}	POC_{phyto}	Derived from counts	
Total phytoplankton-derived particulate organic carbon	mg m^{-3}	$TPOC_{phyto}$	Derived from counts	

to obtain the reduced dimension matrices that fit the data best, determined from the pigment in the model and smallest root mean square (RMS) of the residuals (for more details on CHEMTAX statistics, see (Fragoso et al., 2017)). For CHEMTAX analyses, *in vitro* chlorophyll *a* derived from HPLC analysis ($Chla_{HPLC}$) and the following accessory pigments were chosen because they are considered appropriate markers of many phytoplankton groups: 19-butanoyloxyfucoxanthin (*But-fuco*), 19-hexanoyloxy-4-ketofucoxanthin (*Hex-kfuco*), 19-hexanoyloxyfucoxanthin (*Hex-fuco*), alloxanthin (*Allo*), chlorophyll *b* (*Chl b*), chlorophyll c_1+c_2 (*Chl c_1+c_2*), chlorophyll c_3 (*Chl c_3*), fucoxanthin (*Fuco*), neoxanthin (*Neo*), peridinin (*Peri*) and prasinoxanthin (*Pras*). A complete list

of pigments used in this study and their distributions in algal groups are found in Table 2.

Before running CHEMTAX, initial pigment ratios for each phytoplankton group were carefully selected based on microscopic observations to ensure that matrices are applied and interpreted correctly (Irigoien et al., 2004). Initial pigment ratio tables were based on the geometric means of cultured phytoplankton groups exposed to a variety of E_{PAR} derived from the literature (Higgins et al., 2011) (https://data.aad.gov.au/metadata/records/CHEMTAX). Because of the temporal variation in phytoplankton groups (as observed by microscopic approaches), the distinct initial pigment ratios were applied for three distinct physical and, consequently, irradiance regimes as described in Section 3.1.

CHEMTAX is sensitive to the input values of the initial ratio matrix (Latasa, 2007), therefore, the average of the six best output matrices (with the smallest residuals) were chosen from 60 randomly generated pigment ratio tables (equivalent to 10%) (see Wright et al. (2009) for details). To obtain more stable output matrices, a second re-run of the best output matrices randomly generated was performed to further reduce the RMS (see input matrices and RMS values in Table S2, supplementary material).

To investigate the use of photoprotective carotenoids once cells are exposed to high light levels, carotenoids from the xanthophyll cycle, diadinoxanthin (*DD*) and diatoxanthin (*DT*) were quantified. The ratios of epoxidized (*DD*) and de-epoxidized (*DT*) forms to total HPLC-derived

Table 2

List of phytoplankton pigments and their distributions in algae groups, abbreviations and formulas. PSC = photosynthetic carotenoid, PPC = photoprotective carotenoid, PPP = photosynthetic pigment.

Abbreviation	Name	Type	Present in/Index of/Formula
But-fuco	19′-butanoyloxyfucoxanthin	PSC	Prymnesiophytes, crysophytes and dinoflagellates Type 2* (lacking Peridinin)
Hex-fuco	19′-hexanoyloxyfucoxanthin	PSC	Major in prymnesiophytes and dinoflagellates Type 2* (lacking Peridinin)
Hex-kfuco	19′-hexanoyloxy-4-ketofucoxanthin	PSC	haptophytes Type 5–8*.
Allo	Alloxanthin	PPC	Cryptophytes
$Chla_{HPLC}$	HPLC-derived chlorophyll *a*	PPP	All phytoplankton except *Prochlorococcus*
Chl b	Chlorophyll *b*	PPP	Chlorophytes, prasinophytes, euglenophytes
Chl c_1 + c_2	Chlorophyll c_1 + c_2	PPP	Diatoms, prymnesiophytes, dinoflagellates, cryptophytes, chrysophytes and raphidophytes
Chl c_3	Chlorophyll c_3	PPP	Prymnesiophytes, chrysophytes and dinoflagellates Type 2* (lacking Peridinin)
DD	Diadinoxanthin	PPC	Diatoms, prymnesiophytes, dinoflagellates, chrysophytes and raphidophytes
DT	Diatoxanthin	PPC	Diatoms, prymnesiophytes, dinoflagellates, chrysophytes and raphidophytes
Fuco	Fucoxanthin	PSC	Diatoms, prymnesiophytes, chysophytes, pelagophytes and dinoflagellates Type 2* (lacking Peridinin)
Neo	Neoxanthin		Chlorophytes Type 1*, Prasinophytes Type 1, 2 and 3*, Euglenophytes Type 1*
Peri	Peridinin	PSC	Dinoflagellates Type 1*
Pras	Prasinoxanthin	PPC	Prasinophytes Type 3*

According to Jeffrey et al. (1997) or *Higgins et al. (2011).

chlorophyll *a* biomass (*Chla$_{HPLC}$*) were calculated as *(DD+DT)/Chla$_{HPLC}$* to quantify the amount of photoprotective pigments relative to biomass (Griffith and Vennell, 2010). The de-epoxidation state is an indicator of fast activation of photoprotection under high light and was calculated as *DT/(DD+DT)* (Griffith and Vennell, 2010; Lavaud et al., 2004).

2.7. Carbon and nitrogen analyses

Frozen GF/F filters were placed into clean glass tubes, fumed with HCl acid 37% in a closed box for 30 min, air dried and kept dehydrated. The day before the analyses, filters were packed in 5×9 mm tin capsules (Säntis Analytical, AG) and placed in a microplate. Samples were dried overnight at 60 °C and analyzed for elemental analyses on a Elementar Vario EL Cube (Elementar Analysensysteme GmbH, Hanau, Germany) using acetanilide Sigma Aldrich 00401-5G as a reference.

2.8. Phytoplankton identification and enumeration

Phytoplankton taxonomic identification and counts were only conducted for samples from station B, where Lugol-preserved samples from the upper 5 m and 15 m were combined. Aliquots of 10 ml from the pooled water samples were sedimented in Utermöhl chambers and analyzed using a Nikon Eclipse 100 inverted microscope with × 100–400 magnification. When phytoplankton numbers were generally low, a 25 ml aliquot was sedimented. For the most abundant species, random fields were counted, and the average number of cells was corrected using the ratio of area counted to the area of the whole counting chamber. For rare species, the whole area was examined and counted. Phytoplankton were identified to genus or species, according to Throndsen et al. (2007) and Tomas (1997). Fixed net hauls were, sometimes, used to scan the population composition and to verify the presence of e.g. coccolithophorids, which may be conserved better in formalin-fixed samples.

2.9. Phytoplankton biovolume and carbon biomass estimation

Cell biovolume (based on average size class) and biomass (calculated from pg C cell^{-1}) were estimated according to Olenina et al. (2006). To estimate phytoplankton-derived organic carbon biomass (*POC$_{phyto}$*, mg C m^{-3}), cellular C was multipied by their respective abundance in each sample.

2.10. Statistical analyses

Multivariate analyses were performed on biological and environmental data using PRIMER-E (version 7) software (Clarke and Warwick, 2001). Relative carbon and chlorophyll *a* biomasses of each algal group and pigment concentrations (after log-transformation to increase the importance of rare groups and pigments) were displayed with the associated hydrographic regimes using 'Shade Plot task' in the PRIMER-E software. Coherent plot curves were constructed to identify the major taxa that were associated with each other by exhibiting similar abundance patterns across sampling dates ($p < 0.05$) (Somerfield and Clarke, 2013). For that, the 9 most statistically significant taxa, including diatoms, dinoflagellates and haptophytes that exhibited patterns of co-association, were selected using the 'Coherent plot' task in the PRIMER-E software. These plots were based on calculating similarities (index of association) that exclude joint absences between a pair of taxa (27 in total identified up to species or genus level) (Somerfield and Clarke, 2013) and is represented as the relative taxa abundance (standardized to the total taxa) occurring in distinct sampling dates.

A redundancy analysis (RDA) was performed using the CANOCO 4.5 software (CANOCO, Microcomputer Power, Ithaca, NY). This analysis generates an ordination diagram that best explains the effect of environmental variables (explanatory variables) on the distribution of the phytoplankton groups in Mausund Bank based on CHEMTAX approach.

Environmental variables that significantly explained phytoplankton groups distribution ($p < 0.05$) were analyzed individually (λ_1, marginal effects) and with other forward-selected variables (λa, conditional effects) using 'Forward-selection' task and Monte Carlo permutation test (n = 999, reduced model). More information about this analysis can be found in Fragoso et al. (2016).

3. Results

3.1. Environmental variables from the moored buoy

Temperature and salinity measurements from the moored buoy varied in depth and time. Water temperature within the upper 60 m generally increased with time (average 8–13 °C) and the water column was thermally stratified with the surface typically having the warmest temperature (Fig. 2a). The upper part was only weakly stratified during the beginning of the season, becoming generally fresher over the course of season, particularly at 1 m depth (Fig. 2b).

In the first period of the study (from May to beginning of June) the water column was weakly stratified with potential for being well mixed, herein defined as the 'mixing period' (MP) (average Stratification Index,
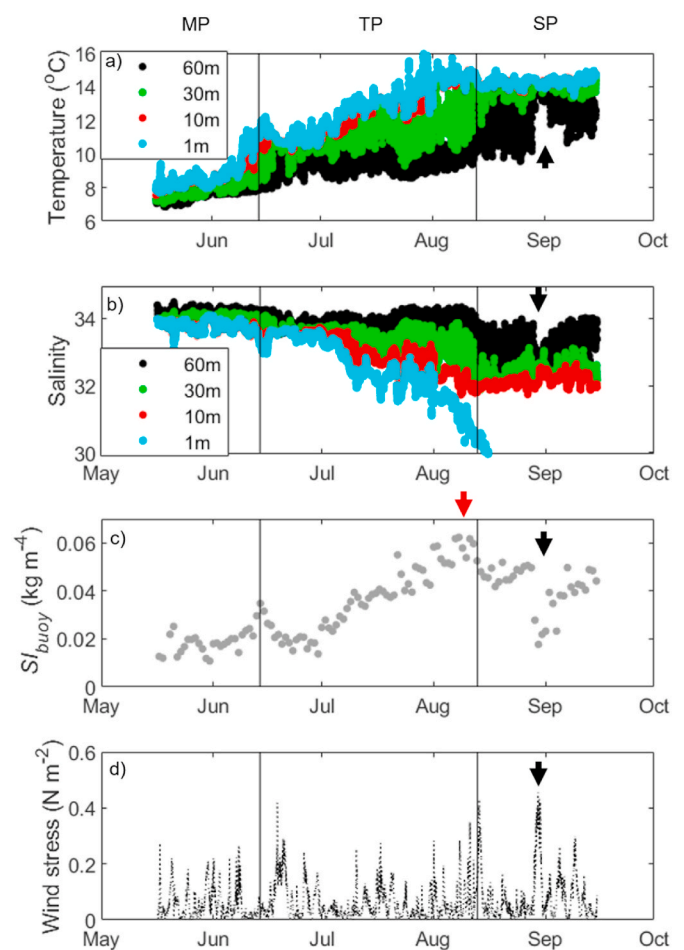

Fig. 2. Buoy data collected for a) temperature and b) salinity at different depths: 1 m, 10 m, 30 m, 60 m, c) maximum daily stratification index (*SI$_{buoy}$*, kg m^{-4}) and wind stress (N m^{-2}) from 16th May to 15th September 2017. Vertical lines indicate periods of hydrodynamic forcing defined as mixing (MP, mid-May to mid-June), transition (TP, mid-June to mid-August) and stratified period (SP, mid-August to mid-September). Note the highest stratification value at the beginning of August (red arrow) and the disruption of stratification in the end of August/beginning of September due to strong wind stress (black arrow). (For interpretation of the references to color in this figure legend, the reader is referred to the Web version of this article.)

SI_{buoy} = 0.02 kg m^{-4}) (Fig. 2c). Stratification gradually increased from 0.02 to 0.06 kg m^{-4} over the summer (mid-June to mid-August) and this period was defined as the 'transition period' (TP) (Fig. 2c). During the last period of study (from mid-August until late September), stratification was more established (around 0.05 kg m^{-4}), except at the end of August/beginning of September, when it was broken by a mixing event (SI_{buoy} values decreased to 0.02 kg m^{-4}, Fig. 2c) caused by strong winds (wind stress = 0.48 N m^{-2}) (Fig. 2d). This period was defined as the 'stratified period' (SP).

3.2. Environmental variables from field cruises

Similar to the data obtained from the moored buoy, potential density ($\sigma_{\theta,}$ calculated as a function of temperature and salinity from vertical profiles from the boat) varied with depth and time over the duration of the study (late April until late September), but with less variation between stations A and B (Fig. 3a and b, Fig. S1, supplementary material). Generally, the upper 50 m became less dense with time, where a fresh buoyant surface layer (σ_{θ} < 25 kg m^{-3}) became thicker from TP to SP (Fig. 3a and b). The low density of the surface layer contributed to relatively strong vertical stratification, which was observed by positive Brunt-Väisälä Frequency values (N^2> 0.0001 s^{-1}), with the highest values (N^2> 0.001 s^{-1}) observed in mid-August throughout the upper 50 m (Fig. 3c and d). During the SP, stratification was observed to be stronger in deeper waters (35–80 m) because of the thickening of the fresh buoyant layer, however, the surface waters presented low/negative N^2 values in the end August/beginning September, suggesting disruption of stratification in the upper 40 m (Fig. 3b and d).

Surface (<15 m) nutrient concentrations ([NO$_3$], [PO$_4$] and [SiOH$_4$]) varied noticeably with time, except for [NH$_4$], which showed random surges (concentrations > 1 μM) throughout the period of study (Fig. 4a). In general, [PO$_4$] and [NO$_3$] was slightly higher at station A than B (Fig. 4b and c). Nutrients peaked in the MP ([NO$_3$] ~ 3.0 μM, [PO$_4$] ~ 0.27 μM, [SiOH$_4$] up to 3 μM), decreased gradually over time with lowest values at the end of the TP ([NO$_3$] and [SiOH$_4$] < 0.5 μM, [PO$_4$] ~ 0.06 μM), and increased again, particularly [SiOH$_4$] (>0.5 μM) during the SP (Fig. 4b–d).

3.3. Pigment data and phytoplankton carbon and chlorophyll a biomass

Concentrations of pigment markers as well as phytoplankton community composition derived from carbon conversion of cell counts and CHEMTAX agreed well, in general, for some groups (Fig. 5). Diatom biomasses (in terms of C and $Chla_{CHEMTAX}$) peaked in the MP, at the end of TP and in some stages of the SP (Fig. 5a and b). This trend was also confirmed through high concentrations of *Fuco* (Fig. 5c). Dinoflagellates (in terms of C and [$Chla_{CHEMTAX}$]) were present throughout the whole study (Fig. 5a and b), although the species that contain *Peri* were more abundant during the MP and sometimes in the SP (Fig. 5c). Other flagellates, such as cryptophytes, euglenoids and prasinophytes, have pigment-specific markers (*Allo*, *Neo*, *Pras*, respectively). These flagellates, in addition to non-identified pico- or nanoflagellates, had higher C biomass towards the end of the study, in the SP (Fig. 5a), although accuracy in counts was difficult via microscopic approaches because of their minute size. To complement this information, pigment approaches were necessary and showed an increase in biomass ($Chla_{CHEMTAX}$) of main flagellate groups, such as prasinophytes and haptophytes towards the end of the season (Fig. 5b and c).

3.4. Phytoplankton species composition

Coherent plots of major identified taxa showed species associations occurring during the three distinct physical regimes (MP, TP, SP). The diatom *Skeletonema costatum* occurred mostly during the MP (Fig. 6a), where a bloom dominated by this species was observed (1.28 × 10^6 cells L^{-1} on 11th May, see Table S3, supplementary material). Towards the end of the TP, *Guinardia delicatula* and *Proboscia alata* were uniquely present, suggesting that these species were indicative of a highly stratified water mass in the end of summer (Fig. 6a). In terms of abundance, however, the most numerous diatom species were *Chaetoceros* spp. (1.63 × 10^5 cells L^{-1}), *G. delicatula* (2.94 × 10^5 cells L^{-1}) and *S. costatum* (1.56 × 10^5 cells L^{-1}) during the end of the TP (Table S3, supplementary material). Diatom cell abundance was generally low during the SP (Table S3, supplementary material), when compared to the other two periods, except for *Pseudo-nitzschia* spp. and *Cylindrotheca closterium*, which appeared mostly during mid-September (Fig. 6a).

The small-sized, *Peri*-containing dinoflagellate, *Heterocapsa rotundata*, was predominant during the MP (Fig. 6b), forming a bloom around 11th May (2.47 × 10^4 cells L^{-1}) (Table S3, supplementary material). In terms of abundance, dinoflagellates were generally low during the TP (Table S3, supplementary material), although the genus *Tripos* spp. was persistently present during this period (Fig. 6b). There was also an increased abundance of unidentified cells of *Gyrodinium/Gymnodinium*-types in the SP (3.78 × 10^4 cells L^{-1} on 7th September). This was
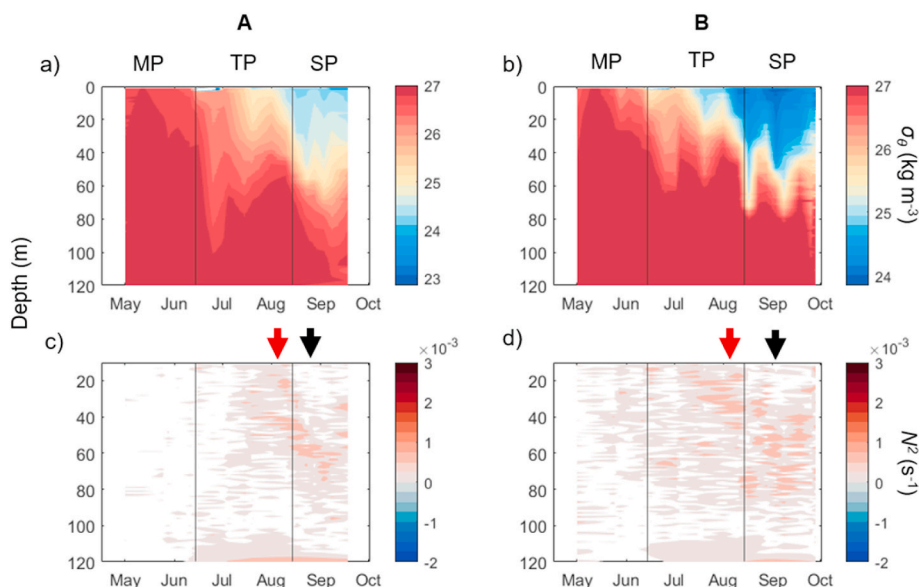

Fig. 3. Vertical profiles of a, b) density (σ_{θ}, kg m^{-3}) and c, d) Brunt-Väisälä frequency (N^2, s^{-1}) in stations A (left) and B (right) derived from CTD measurements during field campaigns from 30th April to 27th September 2017. Highlighted areas in c) and d) show values where N^2 were positive (>0.0001), suggesting vertical stratification. Vertical lines indicate periods of hydrodynamic forcing defined as mixing (MP, April to mid-June), transition (TP, mid-June to mid-August) and stratified period (SP, mid-August to mid-September). Note the highest stratification throughout the column at the beginning of August (red arrow) and the disruption of stratification of the upper 40 m in the end of August/beginning of September (black arrow). (For interpretation of the references to color in this figure legend, the reader is referred to the Web version of this article.)
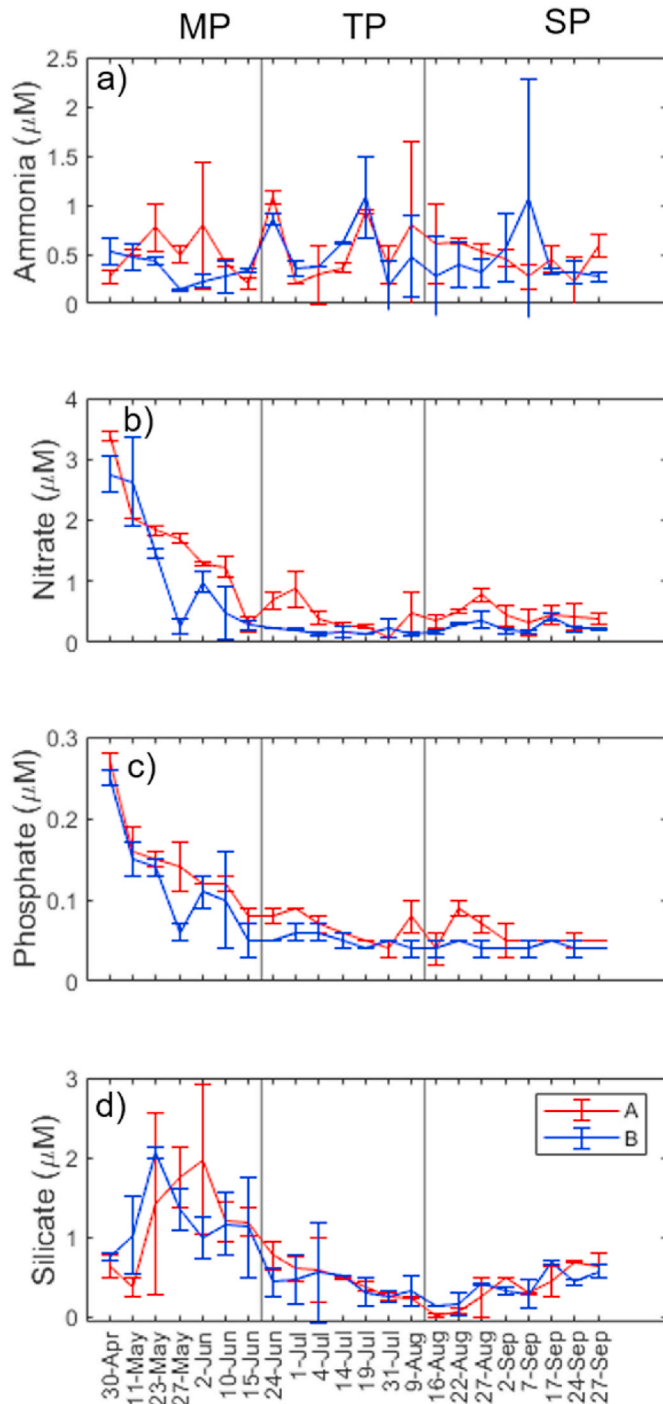
Fig. 4. Nutrient concentrations (in μM), including a) ammonium, b) nitrate, c) phosphate and b) silicate from discrete water sampling at stations A and B. Vertical lines indicate periods of hydrodynamic forcing defined as mixing (MP, mid-May to mid-June), transition (TP, mid-June to mid-August) and stratified period (SP, mid-August to mid-September).
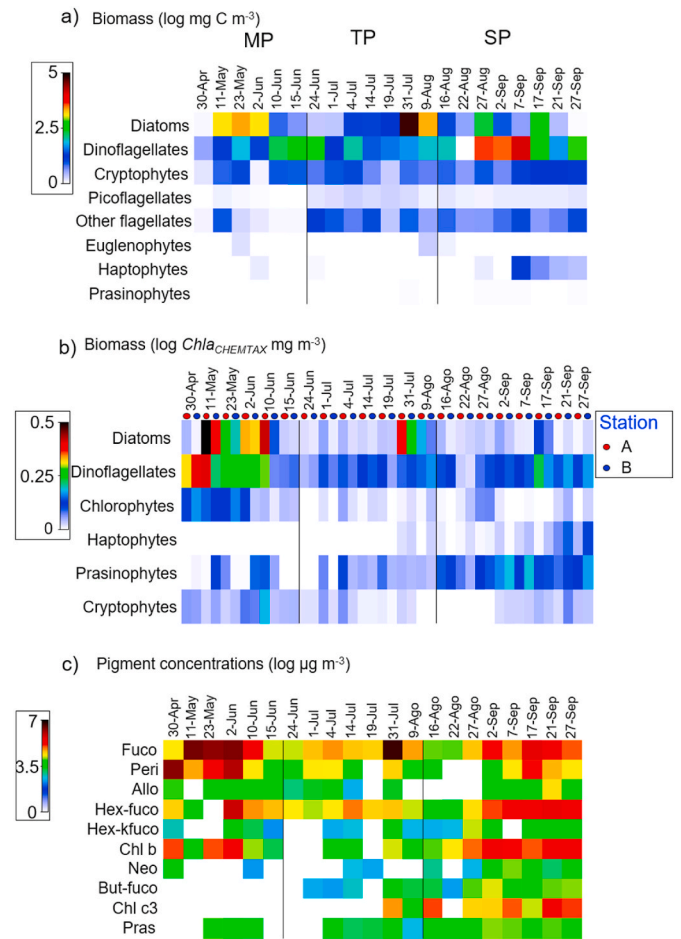

Fig. 5. Shade plot showing the biomass concentrations, in terms of a) carbon (derived from microscopic counts) and b) chlorophyll a from pigment estimations from CHEMTAX ($Chla_{CHEMTAX}$), in addition to c) pigment markers of phytoplankton groups from the upper 15 m at stations B only (a and c) or from stations A and B (b) from the end of April to end of September 2017. All data were log-transformed to increase the importance of non-abundant groups/pigments. Vertical lines indicate periods of hydrodynamic forcing defined as mixing (MP, mid-May to mid-June), transition (TP, mid-June to mid-August) and stratified period (SP, mid-August to mid-September). (For interpretation of the references to color in this figure legend, the reader is referred to the Web version of this article.)

coincident with high amounts of fucoxanthins, consistent with descriptions of dinoflagellates type 2 of the order *Gymnodiniales/Gyrodiniales* (Higgins et al., 2011). A coccolithophore species (haptophyte), possibly *Pleurochrysis* cf., was only observed in high abundance towards the end of the study period, particularly during the SP (Fig. 6b).

3.5. Description of correlations

In general, values of $Chla_{in-vitro}$ and $Fchla$ (median of the respective day when $Chla_{in-vitro}$ was collected) had a good agreement, explaining 47% of the relationship (Fig. S2, supplementary material), in spite of the expected variability of $Fchla$ signal due to photo-physiological response to light regimes. Likewise, POC and bbp (median of the respective day) presented a positive relationship ($R^2 = 0.44$, $p = 0.007$, Fig. S2, supplementary material), although minerals and other inorganic particles also contributed to the bbp pool. When total POC_{phyto} ($TPOC_{phyto}$) were compared to bbp values (median of the respective day), a positive relationship was observed ($R^2 = 0.51$, $p = 0.004$), suggesting that phytoplankton contributed to a significant part of the bbp pool (Fig. S2, supplementary material). Estimations of $TPOC_{phyto}$ was used to investigate the relationship of diatom to flagellate ratios with changes in the ratio of $Fchla$ to bbp. A negative relationship was observed, where low $Fchla:bbp$ ratios occurred in waters of high dominance of diatoms (>50%) (Fig. 7b).

3.6. Optical community index

In general, the optical parameters ($Fchla$, bbp and $Fchla:bbp$) and index (diatom:flagellate, derived from the $TPOC_{phyto}$ and $Fchla:bbp$
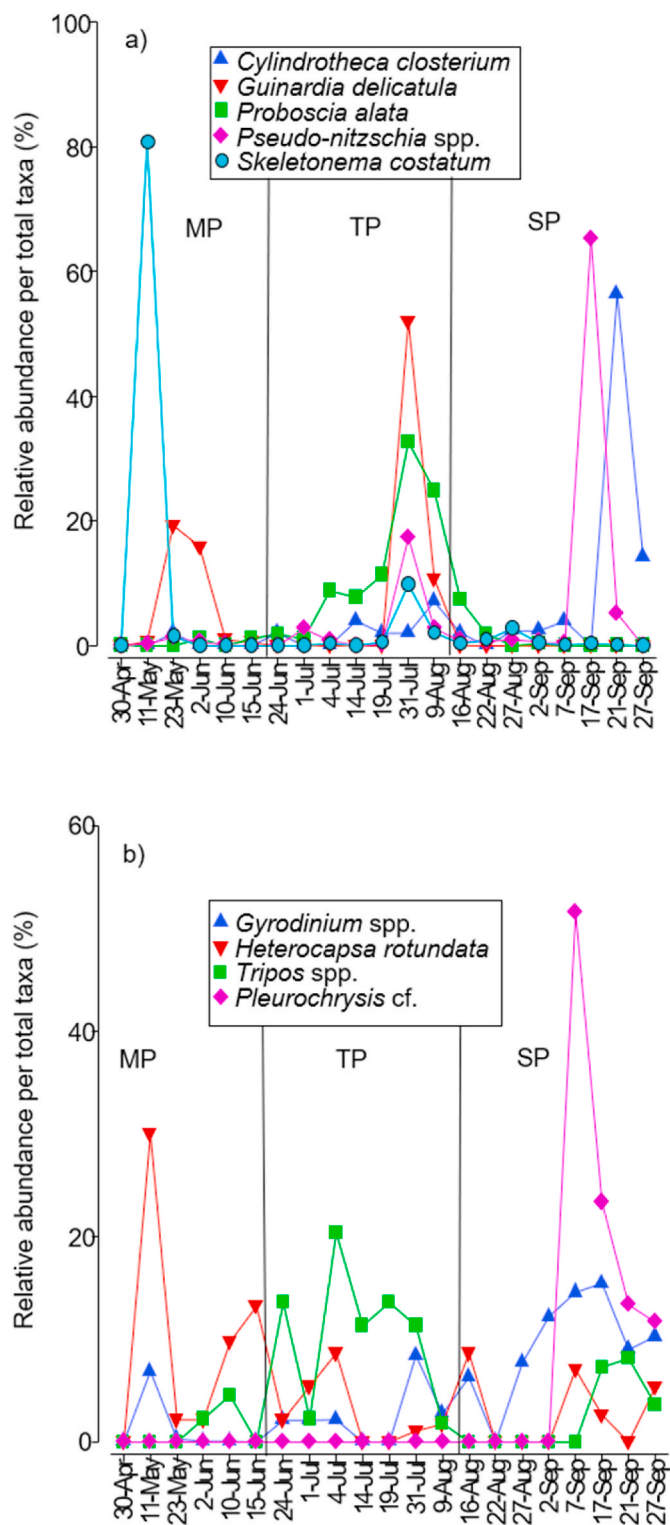
Fig. 6. Coherent species plot showing the relative abundance of the most significant taxa of a) diatoms and b) dinoflagellates and the haptophyte *Pleurochrysis* cf. per total respective taxa from the end of April to end of September 2017. Vertical lines indicate periods of hydrodynamic forcing defined as mixing (MP, mid-May to mid-June), transition (TP, mid-June to mid-August) and stratified period (SP, mid-August to mid-September).
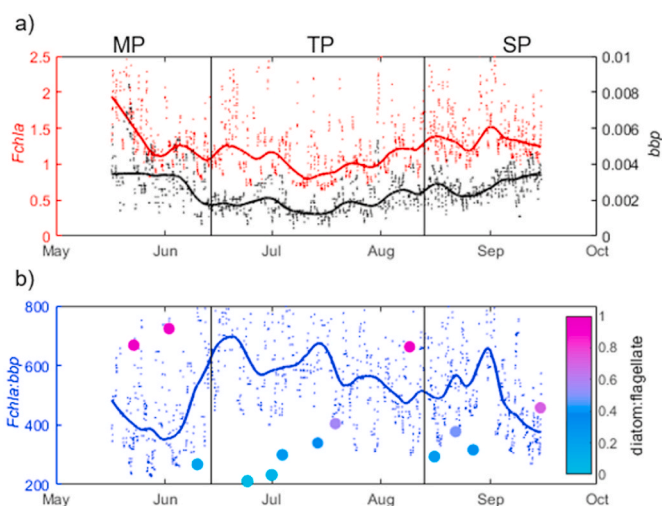

Fig. 7. Buoy data, including a) *in situ* chlorophyll *a* fluorescence (*Fchla*, mg m^{-3}, left axis, red line) and *in situ* particulate backscattering coefficient (*bbp*, m^{-1}, right axis, black) from buoy measurements, in addition to b) the ratio of these two measurements (*Fchla:bbp*, (mg m^{-4}), left axis, blue line) and diatom: flagellate ratio from optical index-derived calculation (right axis, colorbar). Vertical lines indicate periods of hydrodynamic forcing defined as mixing (MP, mid-May to mid-June), transition (TP, mid-June to mid-August) and stratified period (SP, mid-August to mid-September). Dots represent median-calculated data (from seven consecutive runs) and the superimposed line is a smoothing parameter (*rloess* method in Matlab). (For interpretation of the references to color in this figure legend, the reader is referred to the Web version of this article.)

relationship), were not linear, oscillating up and down within days and weeks during the period of the study (Fig. 7). For *Fchla* and *bbp*, both parameters followed similar trends, being relatively high from mid-May until mid-Jun (mixing period, MP), decreasing gradually until reaching the lowest value at the beginning of August (SP) and gradually increasing again afterwards (Fig. 7a). The ratio of these parameters (*Fchla:bbp*), however, was low in the beginning of the study (MP), rapidly increasing in the beginning of July (also the beginning of the SP) and decreasing with time, until it peaked again in the beginning of September and decreased once again towards the end of the study period (Fig. 7b, Fig. S3, supplementary material). Diatom:flagellate, evidently, had opposite trends than *Fchla:bbp*, being high during May and June (MP), weakening during the beginning of SP and gradually increasing during the end of this period, weakening again in September and slightly increasing afterwards (Fig. 7b).

3.7. Environmental controls on phytoplankton size structure

Environmental variables that most explained the variance (explanatory variables) of phytoplankton group distributions (biomass derived from CHEMTAX) were [Si(OH)$_4$], [NO$_3$] and photoperiod (Fig. 8, Table S4, supplementary material). According to the ordination diagram originated from the RDA, dinoflagellates correlated with high [NO$_3$] and diatoms with high [Si(OH)$_4$] (Fig. 8). This is possibly because the former group peaked in the beginning of the MP, when [NO$_3$] was highest (Figs. 4b and 5b), whereas diatoms (also with high biomass during the MP), peaked with a surge of [Si(OH)$_4$] (possibly belonging to a second spring bloom peak) (Figs. 4d and 5b). Conversely, flagellates, such as haptophytes and prasinophytes were dominant in the SP and correlated negatively with photoperiod (p < 0.05) and positively with temperature and stratification (analyzed as the integrated N^2 values from the upper 80 m), although this relationship was not significant (p > 0.05) (Fig. 8, Table S4, supplementary material). Concomitantly, average ratios of the de-epoxidized state of photoprotective carotenoids of the xanthophyll cycle, such as *DT/(DD+DT)* (supplementary variables), increased with
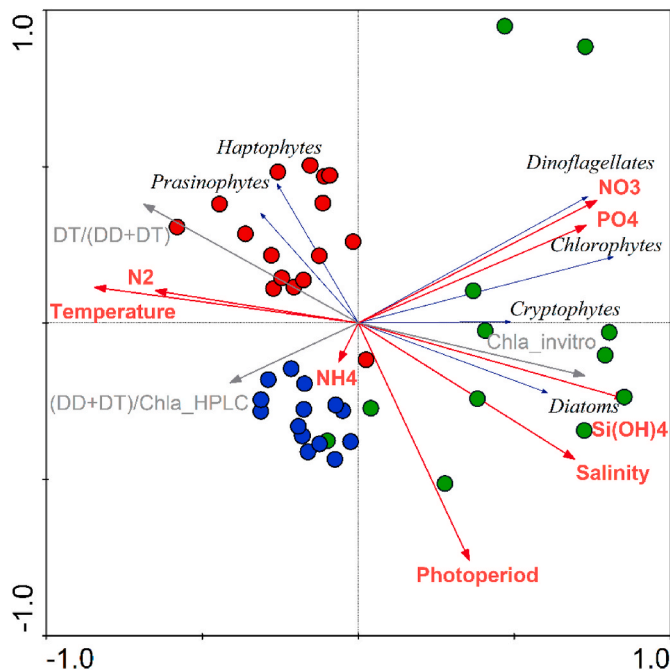
Fig. 8. Ordination diagram generated from redundancy analysis (RDA) with triplot representing data from field work. Biological variables are phytoplankton chlorophyll *a* biomass per group (derived from CHEMTAX approach): diatoms, dinoflagellates, chlorophytes, cryptophytes, haptophytes and prasinophytes (thin, blue arrows), environmental data: nitrate (NO3), phosphate (PO4), silicate (Si(OH)4, μM), salinity, temperature (°C), integrated Brunt-Väisälä frequency values from the upper 80 m (N^2, s^{-1}) and photoperiod (hours) (red arrows) and supplementary variables (light grey arrows): DD = diadinoxanthin, DT = diatoxanthin, Chla_HPLC = HPLC-derived chlorophyll *a*, Chla_invitro = *in-vitro* fluorometric-derived chlorophyll *a*. Closed circles refer to stations sampled in distinct periods (mixing - green) transition - blue and stratified – red, see Fig. 2 for respective dates of each period). (For interpretation of the references to color in this figure legend, the reader is referred to the Web version of this article.)

season (Fig. S4, supplementary material) and also correlated positively with haptophytes and prasinophytes of the SP (Fig. 8). Xanthophyll pigments per chlorophyll *a* (referred as *(DD+DT)/Chla$_{HPLC}$*)) were higher during summer when stratification was building up and [NH$_4$] were, on average, slightly high (Fig. 4a and 8), although this relationship was not significant (Table S4, supplementary material).

4. Discussion

4.1. Using optical indexes for phytoplankton

In this study, patterns of chlorophyll fluorescence (obtained from in *situ Fchla*) and particulate backscattering coefficient (*bbp*) presented, in general, similar trends, being relatively high in the MP, decreasing gradually in the TP and gradually increasing again afterwards during the SP. Such patterns, where an increase in *Fchla* corresponds to a simultaneous increase in *bbp* (and vice-versa), seem to be a common feature of regions with strong seasonality (e.g. North subpolar gyre and the Southern Ocean, Barbieux et al., 2018), including Mausund Bank. Despite being adjusted for *NPq* and biofouling, *Fchla* signal showed a greater fluctuation compared to *bbp*, suggesting that other processes that interfere with light regime, such as tidal oscillations, might be contributing to this variability (Carberry et al., 2019). Variations in tidal current speeds, semi-diurnal (two tidal peaks per day) and spring-neap cycles (two tidal maxima within a month period) have accounted for great variability in the fluorescence signal (Blauw et al., 2012) and were also observed during this study. This occur because tidal advection

changes in chlorophyll *a* biomass (and thus the *Fchla* signal), as well as community structure, occur to such an extent that low tide is associated with the upstream phytoplankton population and high tide is associated with downstream (oceanic) population in near-shore areas (Carberry et al., 2019).

The use of optical index through either *Fchla* or optical backscattering measurements has been suggested as a proxy of phytoplankton community composition in marine systems (Nencioli et al., 2010; Strutton et al., 2011). More recently, Cetinić et al. (2015) observed a positive relationship between diatom:flagellate and *Fchla:bbp*, and suggested this relationship as a new tool for automated determination of phytoplankton taxonomy in clear waters of the North Atlantic. High *Fchla:bbp* was also observed in the North subpolar gyre and Southern Ocean, in waters where microphytoplankton is known to dominate, whereas the low *Fchla:bbp* is found in oligotrophic waters (Barbieux et al., 2018). However, in this study, we observed an opposite trend, where low *Fchla:bbp* was related to high diatom:flagellate. The explanation for low *Fchla* to *bbp* could be that diatoms, which are larger than flagellates, can contribute significantly to a high *bbp* signal (Shang et al., 2014). Moreover, high diatom concentrations during a spring bloom at Mausund Bank are also associated with abundant zooplankton, fecal pellets and marine snow (Fragoso et al., 2019a). Non-algal particles, including fecal pellets and debris have shown to contribute largely to the *bbp* signal, particularly in regions of high chlorophyll *a* biomass (Bella-cicco et al., 2018) and could explain the large fraction of the *bbp* signal in Mausund Bank. In this study, the relationship between *TPOC$_{phyto}$* and *bbp* explained only 51% of the variability, suggesting that other non-algal sources of particles could contribute to the *bbp* pool. Thus, in spite of the negative relationship observed between *Fchla:bbp* and diatom:flagellate, this interpretation can be biased, given that non-algal particles (copepods and fecal pellets) that contribute to the *bbp* pool are associated with diatom blooms, making this hypothesis refutable in productive coastal regions where secondary production is tightly coupled with phytoplankton blooms, such as Mausund on the coast of Norway.

Regardless, the variability of *Fchla:bbp* in the Mausund Bank was highly seasonal and likely reflected the changes that distinct hydrographic regimes cause in phytoplankton community composition and physiology, zooplankton abundances, and marine snow or other mineral particle concentrations. For that reason, we suggest that the use of this optical proxy for detecting phytoplankton functional groups in coastal, highly productive areas, such as Mausund Bank, is not suitable to be used alone, even though a negative relationship was found. Under this circumstance, using other sensors such as *in situ* flow cytometer (Sosik and Olson, 2007) and silhouette camera (Fragoso et al., 2019a) that are able to categorize particle types could be used to refine the proxy in these highly productive coastal regions.

4.2. Environmental/physical forcing over phytoplankton community succession

Changes in biomass (both in terms of *Chla$_{CHEMTAX}$* and *POC$_{phyto}$*), in addition to the succession of phytoplankton (species and groups) were observed during the period of study (end of April until end of September 2017) at Mausund Bank. This was caused by changes in the physical settings (along with nutrients and light levels) as the seasons progressed, such as a more mixed environment in spring, an onset of stratification in summer and sporadic strong winds causing disruption of a thick, stratified layer during fall. Nutrient availability during pre-bloom conditions, in combination with increased irradiance in March have shown to promote the spring bloom in the mid-coast of Norway, including Trondheimsfjord (Sakshaug and Myklestad, 1973) and Frøya (another island near Mausund) (Magnesen and Christophersen, 2008). Similar to observations in Trondheimsfjord, a second peak of the spring bloom was observed in mid-May in Mausund Bank and was associated with a transient increase in silicate concentration (Sakshaug and Myklestad, 1973). Internal waves occurring at Mausund Bank flank, which causes a

'lift' of nutrient-rich waters of Atlantic origin, combined with intense tidal mixing over the bank, have been suggested as an additional source of nutrients at the bank (Fragoso et al., 2019a) and could stimulate a second peak bloom observed in Mausund. These events might also account for the prolongation of the spring bloom in Mausund area (until beginning of June), as opposed to other islands in the mid-coast of Norway, where the spring bloom typically dies off weeks before (Throndsen et al., 2007).

Enhanced stratification observed during summer in this study is due to the increased volume of the fresh (less saline) and buoyant Norwegian Coastal Current that moves northwards along the Norwegian coast, carrying freshwater from the Baltic Sea and Norwegian rivers (Christensen et al., 2018). This water mass, therefore, carries a history of high nutrient utilization before it reaches the mid-coast of Norway in summer, with low concentrations (<4 μM for nitrate and <2 μM for silicate) (Rey et al., 2007). The coastal water gets fresher and warmer and the layer gets thicker during summer and fall and the resulting enhanced stratification of upper waters suppresses fluxes of nutrients to the surface. The phytoplankton need, thus, to rely on remineralized nutrients (Rey et al., 2007). This might have selected for small-sized phytoplankton (pico- and nanoflagellates) in surface waters for most of the summer, given that low nutrient concentrations favor smaller phytoplankton due to their greater efficiency in nutrient acquisition (larger surface to volume ratios and smaller diffusion boundary layer) (Litchman and Klausmeier, 2008).

Ability to cope with high and/or continuous light conditions resulting from enhanced water column stratification and longer day-light periods (high $SI_{buoy}*E_{PAR}$ values in this study), might have favored the phytoplankton during summer and early fall as well. Small-sized phytoplankton show fast metabolic repair of photosystem II after photoinactivation compared to larger cells (Key et al., 2010; Kropuenske et al., 2009). Moreover, they can rely on photoprotective carotenoids such as diatoxanthin (*DT*), diadinoxanthin (*DD*), violaxanthin and zeaxanthin under highlight conditions (Polimene et al., 2014). In fact, the concentration of the photoprotective *DT* and *DD* per chlorophyll *a* biomass (*Chla$_{HPLC}$*), increased in summer, whereas the de-epoxidized form, *DT*, was higher in early fall, suggesting that the cells were potentially being exposed to continuous, high irradiances (Griffith and Vennell, 2010).

Towards the end of the study season (SP), the stratification of the thick surface layer was broken down in the end of August/beginning of September and at the same time phytoplankton concentrations were observed to increase again. Fall blooms are less reported, particularly in the coast of Norway, although they have been observed in northern fjords (Eilertsen and Frantzen, 2007) and the southern coast of Norway (Dahl and Johannessen, 1998). These blooms seem to be triggered by strong winds, which break down the stratification, allowing an increased vertical flux of nutrient from deeper waters, while irradiance is still sufficient for growth (Eilertsen and Frantzen, 2007). It is possible that a similar event happened at Mausund Bank, where strong winds caused disruption of stratification in the fall that might have re-introduced nutrients (particularly silicate, in this study) and contributed to an increase in phytoplankton biomass, though not with the same intensity as observed in spring.

Based on pigment and taxonomic approaches, phytoplankton groups from Mausund Bank varied according to season, where, in general, diatoms peaked in May (MP), were high in biomass towards the end of the TP (end of July) and reappeared sporadically in mid-September. Intense tidal mixing in the shallow bank and spore inoculum from the seafloor, in addition to the high silicate concentrations in May (compared to the rest of the season) explained the presence of spore-forming and overwintering diatoms (*Thalassiosira*, *Chaetoceros* and *Skeletonema*, Table S3, supplementary material) during this period (Gettings et al., 2014). Rhizosolenid diatom species (*Proboscia alata* and *Guinardia delicatula*) were found during contrasting conditions when stratification was at a maximum (end of July/beginning of August). These diatoms are typically known to accumulate in summer stratified conditions (Kemp et al., 2006) and have been observed in thin layers (<5 m) of subsurface chlorophyll *a* maxima during summer in temperate coastal waters (Barnett et al., 2019). Therefore, it is possible that these species have resurfaced from deeper waters, crossing the pycnocline barrier (migration rates up to 6.4 mh^{-1}, Villareal et al., 1993), given their ability to regulate their buoyancy in the water column, allowing them to exploit nutrient supply in deeper waters as well as light at the surface (Woods and Villareal, 2008). The diatoms species that sporadically occurred in September were *Pseudo-nitzschia*, *Cylindrotheca closterium* and *Guinardia flaccida*. Strong wind events observed in the end of August likely contributed to the increase in nutrient concentrations, particularly silicate, and the reappearance of these species in these waters, whereas nitrate and phosphate were rapidly assimilated by other phytoplankton groups. *Pseudo-nitzschia* and *Cylindrotheca closterium*, which are considered 'R strategists' (disturbance-tolerant species), have high aspect ratios (pennates), and this morphology could improve the cell's ability for nutrient uptake and light harvesting, by increasing the spin of cells in a turbulently mixed environment (Alves-de-Souza et al., 2008).

Dinoflagellates, particularly peridinin-containing ones (*Heterocapsa rotundata*) were abundant during the MP (late April until early June) and during the SP, after strong winds in late August, along with diatoms. Meanwhile, fucoxanthin-dominated dinoflagellates were observed in the TP (summer), when consistently increasing stratification was observed. Dinoflagellates, in general, are known to dominate nutrient-poor and thermally stratified waters, given their mixotrophic nature and ability to move to and from the nutricline, which allow them to prey on other organisms and exploit deeper layers of the water column (Aldridge et al., 2014). The dominance of dinoflagellates, including some harmful algae bloom (HAB) species, is consistently observed in thermally stratified waters in the southern coastal areas of Norway and in the North Sea during summer (Bratbak et al., 2011; Johnsen and Sakshaug, 2000). In the mid-coast of Norway, dinoflagellates, particularly *Tripos* spp., also found in this study, have been present in subsurface chlorophyll *a* maxima in July, being an indicative of stratified summer waters (Fossum et al., 2019).

Haptophytes, prasinophytes, euglenoids and other unidentified flagellates were present throughout the whole study, albeit with low biomass (compared to diatoms). In this study, coccolith-bearing haptophytes, possibly *Pleurochrysis* sp., was an indicator species of the SP. *Pleurochrysis* is a typical coastal coccolithophore (Houdan et al., 2004) and blooms, including *Emiliania huxleyi*, are regularly observed along the coast of Norway during summer/early fall (Bratbak et al., 2011). *E. huxleyi* is associated with Atlantic water (Hegseth and Sundfjord, 2008) and is sometimes introduced into fjords (Riebesell et al., 2017), including Trondheimsfjord (Volent et al., 2011).

In this study, we investigated phytoplankton community dynamics using time-series of *in situ* optical and hydrographical measurements from a moored buoy, in addition to discrete observations of phytoplankton functional groups and indicator species from pigment data, chemotaxonomy and microscopy for validation. Hydrographic regimes shaped phytoplankton succession in the region, where 1) intense vertical mixing and high nutrient concentrations in spring favored a bloom dominated by the diatom *Skeletonema costatum*, 2) a gradual increase in stratification allowed the prevalence of flagellates, followed by a bloom of rhizosolenid diatom species (*Proboscia alata* and *Guinardia delicatula*) in summer and 3) episodic strong wind events in fall disrupt the stratification of a thick fresh buoyant layer that, consequently, reintroduced nutrients for a bloom of diatoms, coccolithophores and dinoflagellates. As opposed to what is observed in clear, open ocean waters, low *Fchla*: *bbp* was related to high diatom:flagellate. This occurred possibly because spring diatom blooms are associated with light scattering objects related to zooplankton abundance, fecal pellets and marine snow in Mausund, making productive regions in the coast of Norway not suitable for the application of this proxy.

Authors contributions

G.M.F. and I. E. designed the study and developed the hypothesis. G. M.F. analyzed the buoy and pigment data, performed the statistical analyses and wrote the initial draft of the manuscript. M.S.C. identified, counted the phytoplankton species in the microscope and provided feedback on phytoplankton ecology. I.E. and F.C. analyzed part of the hydrographic data and provided feedback regarding the physical oceanographic aspect of the paper. I.E. and G.J. supervised the study. All authors contributed substantially to posterior drafting of the manuscript, provided critical comments and approved the final submitted version.

Declaration of competing interest

The authors declare that they have no known competing financial interests or personal relationships that could have appeared to influence the work reported in this paper.

Acknowledgements

Appendix A. Supplementary data

Supplementary data to this article can be found online at https://doi.org/10.1016/j.csr.2020.104322.

References

Aldridge, D., Purdie, D.A., Zubkov, M.V., 2014. Growth and survival of Neoceratium hexacanthum and Neoceratium candelabrum under simulated nutrient-depleted conditions. J. Plankton Res. 36, 439–449. https://doi.org/10.1093/plankt/fbt098.

Alves-de-Souza, C., Gonzalez, M.T., Iriarte, J.L., 2008. Functional groups in marine phytoplankton assemblages dominated by diatoms in fjords of southern Chile. J. Plankton Res. 30, 1233–1243. https://doi.org/10.1093/plankt/fbn079.

Barbieux, M., Uitz, J., Bricaud, A., Organelli, E., Poteau, A., Schmechtig, C., Gentili, B., Obolensky, G., Leymarie, E., Penkerc'h, C., D'Ortenzio, F., Claustre, H., 2018. Assessing the variability in the relationship between the particulate backscattering coefficient and the chlorophyll a concentration from a global biogeochemical-argo database. J. Geophys. Res. Ocean. 123, 1229–1250. https://doi.org/10.1002/2017JC013030.

Barnett, M.L., Kemp, A.E.S., Hickman, A.E., Purdie, D.A., 2019. Shelf sea subsurface chlorophyll maximum thin layers have a distinct phytoplankton community structure. Continent. Shelf Res. 174, 140–157. https://doi.org/10.1016/j.csr.2018.12.007.

Beaugrand, G., Reid, P.C., Ibañez, F., Lindley, J.A., Edwards, M., 2002. Reorganization of North Atlantic marine copepod biodiversity and climate. Science 84 296, 1692–1694. https://doi.org/10.1126/science.1071329.

Bellacicco, M., Volpe, G., Briggs, N., Brando, V., Pitarch, J., Landolfi, A., Colella, S., Marullo, S., Santoleri, R., 2018. Global distribution of non-algal particles from ocean color data and implications for phytoplankton biomass detection. Geophys. Res. Lett. 45, 7672–7682. https://doi.org/10.1029/2018GL078185.

Blauw, A.N., Benincà, E., Laane, R.W.P.M., Greenwood, N., Huisman, J., 2012. Dancing with the tides: fluctuations of coastal phytoplankton orchestrated by different oscillatory modes of the tidal cycle. PloS One 7, e49319. https://doi.org/10.1371/journal.pone.0049319.

Bratbak, G., Jacquet, S., Larsen, A., Pettersson, L.H., Sazhin, A.F., Thyrhaug, R., 2011. The plankton community in Norwegian coastal waters—abundance, composition, spatial distribution and diel variation. Continent. Shelf Res. 31, 1500–1514. https://doi.org/10.1016/j.csr.2011.06.014.

Carberry, L., Roesler, C., Drapeau, S., 2019. Correcting in situ chlorophyll fluorescence time-series observations for nonphotochemical quenching and tidal variability reveals nonconservative phytoplankton variability in coastal waters. Limnol Oceanogr. Methods 17, 462–473. https://doi.org/10.1002/lom3.10325.

Cetinić, I., Perry, M.J., Briggs, N.T., Kallin, E., D'Asaro, E.A., Lee, C.M., 2012. Particulate organic carbon and inherent optical properties during 2008 North Atlantic Bloom Experiment. n/a-n/a J. Geophys. Res. Ocean. 117. https://doi.org/10.1029/2011JC007771.

Cetinić, I., Perry, M.J., D&apos, Asaro, E., Briggs, N., Poulton, N., Sieracki, M.E., Lee, C. M., 2015. A simple optical index shows spatial and temporal heterogeneity in phytoplankton community composition during the 2008 North Atlantic Bloom Experiment. Biogeosciences 12, 2179–2194. https://doi.org/10.5194/bg-12-2179-2015.

Christensen, K.H., Sperrevik, A.K., Broström, G., 2018. On the variability in the onset of the Norwegian Coastal Current. J. Phys. Oceanogr. 48, 723–738. https://doi.org/10.1175/JPO-D-17-0117.1.

Clarke, K.R., Warwick, R.M., 2001. Change in Marine Communities: an Approach to Statistical Analysis and Interpretation, second ed. PRIMER-E, Plymouth.

Dahl, E., Johannessen, T., 1998. Temporal and spatial variability of phytoplankton and chlorophylla: lessons from the south coast of Norway and the Skagerrak. ICES J. Mar. Sci. 55, 680–687. https://doi.org/10.1006/jmsc.1998.0401.

Davies, E.J., Nepstad, R., 2017. In situ characterisation of complex suspended particulates surrounding an active submarine tailings placement site in a Norwegian fjord. Reg. Stud. Mar. Sci. 16, 198–207. https://doi.org/10.1016/j.rsma.2017.09.008.

Edwards, K.F., Litchman, E., Klausmeier, C.A., 2013. Functional traits explain phytoplankton community structure and seasonal dynamics in a marine ecosystem. Ecol. Lett. 16, 56–63. https://doi.org/10.1111/ele.12012.

Eilertsen, H.C., Frantzen, S., 2007. Phytoplankton from two sub-Arctic fjords in northern Norway 2002–2004: I. Seasonal variations in chlorophyll a and bloom dynamics. Mar. Biol. Res. 3, 319–332. https://doi.org/10.1080/17451000701632877.

Fossum, T.O., Fragoso, G.M., Davies, E.J., Ullgren, J.E., Mendes, R., Johnsen, G., Ellingsen, I., Eidsvik, J., Ludvigsen, M., Rajan, K., 2019. Toward adaptive robotic sampling of phytoplankton in the coastal ocean. Sci. Robot. 4 https://doi.org/10.1126/scirobotics.aav3041 eaav3041.

Fragoso, G.M., Davies, E.J., Ellingsen, I., Chauton, M.S., Fossum, T.O., Ludvigsen, M., Steinhovden, K.B., Rajan, K., Johnsen, G., 2019a. Physical controls on phytoplankton size structure, photophysiology and suspended particles in a Norwegian biological hotspot. Prog. Oceanogr. 175, 284–299. https://doi.org/10.1016/j.pocean.2019.05.001.

Fragoso, G.M., Poulton, A.J., Pratt, N.J., Johnsen, G., Purdie, D.A., 2019b. Trait-based analysis of subpolar North Atlantic phytoplankton and plastidic ciliate communities using automated flow cytometer. Limnol. Oceanogr. in review. https://doi.org/10.1002/lno.11189 lno.11189.

Fragoso, G.M., Poulton, A.J., Yashayaev, I.M., Head, E.J.H., Purdie, D.A., 2017. Spring phytoplankton communities of the Labrador Sea (2005–2014): pigment signatures, photophysiology and elemental ratios. Biogeosciences 14, 1235–1259. https://doi.org/10.5194/bg-14-1235-2017.

Fragoso, G.M., Poulton, A.J., Yashayaev, I.M., Head, E.J.H., Stinchcombe, M.C., Purdie, D.A., 2016. Biogeographical patterns and environmental controls of phytoplankton communities from contrasting hydrographical zones of the Labrador Sea. Prog. Oceanogr. 141, 212–226. https://doi.org/10.1016/j.pocean.2015.12.007.

Gettings, R.M., Townsend, D.W., Thomas, M.A., Karp-Boss, L., 2014. Dynamics of late spring and summer phytoplankton communities on Georges Bank, with emphasis on diatoms, Alexandrium spp., and other dinoflagellates. Deep Sea Res. Part II Top. Stud. Oceanogr. 103, 120–138. https://doi.org/10.1016/j.dsr2.2013.05.012.

Griffith, G., Vennell, R., 2010. Photoprotection in Southern Ocean phytoplankton: missing key to low primary productivity. Nat. Preced. https://doi.org/10.1038/npre.2010.5377.1.

Hegseth, E.N., Sundfjord, A., 2008. Intrusion and blooming of Atlantic phytoplankton species in the high Arctic. J. Mar. Syst. 74, 108–119. https://doi.org/10.1016/j.jmarsys.2007.11.011.

Higgins, H.W., Wright, S.W., Schlüter, L., 2011. Quantitative interpretation of chemotaxonomic pigment data. In: Roy, S., Llewellyn, C., Egeland, E.S., Johnsen, G. (Eds.), Phytoplankton Pigments: Characterization, Chemotaxonomy and Applications in Oceanography. Cambridge University Press, Cambridge, pp. 257–313. https://doi.org/10.1017/CBO9780511732263.010.

Holm-Hansen, O., Riemann, B., 1978. Chlorophyll a determination: improvements in methodology. Oikos 30, 438. https://doi.org/10.2307/3543338.

Houdan, A., Bonnard, A., Fresnel, J., Fouchard, S., Billard, C., Probert, I., 2004. Toxicity of coastal coccolithophores (prymnesiophyceae, haptophyta). J. Plankton Res. 26, 875–883. https://doi.org/10.1093/plankt/fbh079.

Huot, Y., Babin, M., 2010. Overview of fluorescence protocols: theory, basic concepts, and practice. Chlorophyll a Fluorescence in Aquatic Sciences: Methods and Applications. Springer Netherlands, Dordrecht, pp. 31–74. https://doi.org/10.1007/978-90-481-9268-7_3.

Irigoien, X., Meyer, B., Harris, R., Harbour, D., 2004. Using HPLC pigment analysis to investigate phytoplankton taxonomy: the importance of knowing your species. Helgol. Mar. Res. 58, 77–82. https://doi.org/10.1007/s10152-004-0171-9.

Jeffrey, S.W., Mantoura, R.F.C., Wright, S.W., 1997. Phytoplankton Pigments in Oceanography. SCOR and UNESCO, Paris.

Johnsen, G., Sakshaug, E., 2000. Monitoring of harmful algal blooms along the Norwegian Coast using bio-optical methods. S. Afr. J. Mar. Sci. 22, 309–321. https://doi.org/10.2989/025776100784125726.

Kemp, A.E.S., Pearce, R.B., Grigorov, I., Rance, J., Lange, C.B., Quilty, P., Salter, I., 2006. Production of giant marine diatoms and their export at oceanic frontal zones: implications for Si and C flux from stratified oceans. Global Biogeochem. Cycles 20. https://doi.org/10.1029/2006GB002698 n/a-n/a.

Key, T., McCarthy, A., Campbell, D.A., Six, C., Roy, S., Finkel, Z.V., 2010. Cell size trade-offs govern light exploitation strategies in marine phytoplankton. Environ. Microbiol. 12, 95–104. https://doi.org/10.1111/j.1462-2920.2009.02046.x.

Kropuenske, L.R., Mills, M.M., van Dijken, G.L., Bailey, S., Robinson, D.H., Welschmeyer, N.A., Arrigo, K.R., 2009. Photophysiology in two major Southern Ocean phytoplankton taxa: photoprotection in phaeocystis Antarctica and

fragilariopsis cylindrus. Limnol. Oceanogr. 54, 1176–1196. https://doi.org/10.4319/lo.2009.54.4.1176.

Large, W.G., Pond, S., 1981. open ocean momentum flux measurements in moderate to strong winds. J. Phys. Oceanogr. 11, 324–336. https://doi.org/10.1175/1520-0485(1981)011<0324:OOMFMI>2.0.CO;2.

Latasa, M., 2007. Improving estimations of phytoplankton class abundances using CHEMTAX. Mar. Ecol. Prog. Ser. 329, 13–21. https://doi.org/10.3354/meps329013.

Lavaud, J., Rousseau, B., Etienne, A.L., 2004. General features of photoprotection by energy dissipation in planktonic diatoms (Bacillariophyceae). J. Phycol. 40, 130–137. https://doi.org/10.1046/j.1529-8817.2004.03026.x.

Lehmuskero, A., Skogen Chauton, M., Boström, T., 2018. Light and photosynthetic microalgae: a review of cellular- and molecular-scale optical processes. Prog. Oceanogr. 168, 43–56. https://doi.org/10.1016/j.pocean.2018.09.002.

Litchman, E., Klausmeier, C.A., 2008. Trait-based community ecology of phytoplankton. Annu. Rev. Ecol. Evol. Syst. 39, 615–639. https://doi.org/10.1146/annurev.ecolsys.39.110707.173549.

Mackey, M.D., Mackey, D.J., Higgins, H.W., Wright, S.W., 1996. Chemtax - a program for estimating class abundances from chemical markers: application to HPLC measurements of phytoplankton. Mar. Ecol. Prog. Ser. 144, 265–283.

Magnesen, T., Christophersen, G., 2008. Reproductive cycle and conditioning of translocated scallops (Pecten maximus) from five broodstock populations in Norway. Aquaculture 285, 109–116. https://doi.org/10.1016/j.aquaculture.2008.08.024.

Martin-Platero, A.M., Cleary, B., Kauffman, K., Preheim, S.P., McGillicuddy, D.J., Alm, E. J., Polz, M.F., 2018. High resolution time series reveals cohesive but short-lived communities in coastal plankton. Nat. Commun. 9, 266. https://doi.org/10.1038/s41467-017-02571-4.

Mojica, K.D.A., van de Poll, W.H., Kehoe, M., Huisman, J., Timmermans, K.R., Buma, A. G.J., van der Woerd, H.J., Hahn-Woernle, L., Dijkstra, H.A., Brussaard, C.P.D., 2015. Phytoplankton community structure in relation to vertical stratification along a north-south gradient in the Northeast Atlantic Ocean. Limnol. Oceanogr. 60, 1498–1521. https://doi.org/10.1002/lno.10113.

Nencioli, F., Chang, G., Twardowski, M., Dickey, T.D., 2010. Optical characterization of an eddy-induced diatom bloom west of the island of Hawaii. Biogeosciences 7, 151–162. https://doi.org/10.5194/bg-7-151-2010.

Olenina, I., Hajdu, S., Edler, L., Andersson, A., Wasmund, N., Busch, S., Göbel, J., Gromisz, S., Huseby, S., Huttunen, M., Jaanus, A., Kokkonen, P., Ledaine, I., Niemkiewicz, E., 2006. Biovolumes and size-classes of phytoplankton in the Baltic Sea. In: Baltic Sea Environment Proceedings. HELCOM Balt.Sea Environ. Proc.

Pereira, G.C., Figueiredo, A.R., Ebecken, N.F.F., 2017. Using in situ flow cytometry images of ciliates and dinoflagellates for aquatic system monitoring. Braz. J. Biol. https://doi.org/10.1590/1519-6984.05016.

Polimene, L., Brunet, C., Butenschön, M., Martinez-Vicente, V., Widdicombe, C., Torres, R., Allen, J.I., 2014. Modelling a light-driven phytoplankton succession. J. Plankton Res. 36, 214–229. https://doi.org/10.1093/plankt/fbt086.

Rey, F., Aure, J., Danielssen, D., 2007. Temporal and spatial distribution of nutrients. In: Sætre, R. (Ed.), The Norwegian Coastal Current - Oceanography and Climate. Tapir Academic Press, Trondheim, pp. 73–88.

Reynolds, C.S., 1993. Scales of disturbance and their role in plankton ecology. Hydrobiologia 249, 157–171. https://doi.org/10.1007/BF00008851.

Riebesell, U., Bach, L.T., Bellerby, R.G.J., Monsalve, J.R.B., Boxhammer, T., Czerny, J., Larsen, A., Ludwig, A., Schulz, K.G., 2017. Competitive fitness of a predominant pelagic calcifier impaired by ocean acidification. Nat. Geosci. 10, 19–23. https://doi.org/10.1038/ngeo2854.

Rodríguez, F., Chauton, M., Johnsen, G., Andresen, K., Olsen, L.M., Zapata, M., 2006. Photoacclimation in phytoplankton: implications for biomass estimates, pigment functionality and chemotaxonomy. Mar. Biol. 148, 963–971. https://doi.org/10.1007/s00227-005-0138-7.

Roesler, C., Uitz, J., Claustre, H., Boss, E., Xing, X., Organelli, E., Briggs, N., Bricaud, A., Schmechtig, C., Poteau, A., D'Ortenzio, F., Ras, J., Drapeau, S., Haëntjens, N., Barbieux, M., 2017. Recommendations for obtaining unbiased chlorophyll estimates from in situ chlorophyll fluorometers: a global analysis of WET Labs ECO sensors. Limnol Oceanogr. Methods 15, 572–585. https://doi.org/10.1002/lom3.10185.

Roesler, C.S., 2016. In Situ Chlorophyll Fluorescence Observations on NERACOOS Mooring A01 : Revised Data Flagging and Changing Phenology. Boston.

Sakshaug, E., Myklestad, S., 1973. Studies on the phytoplankton ecology of the trondheimsfjord. III. Dynamics of phytoplankton blooms in relation to environmental factors, bioassay experiments and parameters for the physiological state of the populations. J. Exp. Mar. Biol. Ecol. 11, 157–188. https://doi.org/10.1016/0022-0981(73)90053-1.

Shang, Shaoling, Wu, J., Huang, B., Lin, G., Lee, Z., Liu, J., Shang, Shaoping, 2014. A new approach to discriminate dinoflagellate from diatom blooms from space in the East China Sea. J. Geophys. Res. Ocean. 119, 4653–4668. https://doi.org/10.1002/2014JC009876.

Skagseth, Ø., Drinkwater, K.F., Terrile, E., 2011. Wind- and buoyancy-induced transport of the Norwegian coastal current in the barents sea. J. Geophys. Res. 116, C08007. https://doi.org/10.1029/2011JC006996.

Somerfield, P.J., Clarke, K.R., 2013. Inverse analysis in non-parametric multivariate analyses: distinguishing groups of associated species which covary coherently across samples. J. Exp. Mar. Biol. Ecol. 449, 261–273. https://doi.org/10.1016/j.jembe.2013.10.002.

Sosik, H.M., Olson, R.J., 2007. Automated taxonomic classification of phyoplankton sampled with imaging-in-flow-cytometry. Limnol Oceanogr. Methods 5, 204–216.

Strutton, P.G., Martz, T.R., DeGrandpre, M.D., McGillis, W.R., Drennan, W.M., Boss, E., 2011. Bio-optical observations of the 2004 Labrador Sea phytoplankton bloom. J. Geophys. Res. 116, C11037. https://doi.org/10.1029/2010JC006872.

Sullivan, J.M., Twardowski, M., Zaneveld, J.R., Moore, C., 2013. Measuring optical backscattering in water. In: Kokhanovsky, A.A. (Ed.), Light Scattering Reviews. Springer Berlin Heidelberg, Berlin, pp. 189–224.

Throndsen, J., Hasle, G.R., Tangen, K., 2007. Phytoplankton of Norwegian Coastal Waters. Almater Forlag AS.

Tomas, C.R., 1997. Identifying Marine Phytoplankton. Academic press.

Villareal, T.A., Altabet, M.A., Culver-Rymsza, K., 1993. Nitrogen transport by vertically migrating diatom mats in the North Pacific Ocean. Nature 363, 709–712. https://doi.org/10.1038/363709a0.

Volent, Z., Johnsen, G., Hovland, E.K., Folkestad, A., Olsen, L.M., Tangen, K., Sørensen, K., 2011. Improved monitoring of phytoplankton bloom dynamics in a Norwegian fjord by integrating satellite data, pigment analysis, and Ferrybox data with a coastal observation network. J. Appl. Remote Sens. 5 https://doi.org/10.1117/1.3658032, 053561.

Woods, S., Villareal, T.A., 2008. Intracellular ion concentrations and cell sap density in positively buoyant oceanic phytoplankton. Nova Hedwigia Beih. 133, 131–145.

Wright, S.W., Ishikawa, A., Marchant, H.J., Davidson, A.T., van den Enden, R.L., Nash, G. V., 2009. Composition and significance of picophytoplankton in Antarctic waters. Polar Biol. 32, 797–808. https://doi.org/10.1007/s00300-009-0582-9.

Zapata, M., Rodríguez, F., Garrido, J., 2000. Separation of chlorophylls and carotenoids from marine phytoplankton:a new HPLC method using a reversed phase C8 column and pyridine-containing mobile phases. Mar. Ecol. Prog. Ser. 195, 29–45. https://doi.org/10.3354/meps195029.

Zhang, X., Hu, L., He, M.-X., 2009. Scattering by pure seawater at high salinity. Optic Express 17, 12685. https://doi.org/10.1364/OE.17.012685.